

PROCEEDINGS OF SPIE

SPIDigitalLibrary.org/conference-proceedings-of-spie

Grating-based tomography applications in biomedical engineering

Georg Schulz, Peter Thalmann, Anna Khimchenko, Bert
Müller

SPIE.

Grating-based tomography applications in biomedical engineering

Georg Schulz, Peter Thalmann, Anna Khimchenko and Bert Müller

Biomaterials Science Center, Department of Biomedical Engineering, University of Basel, Switzerland

ABSTRACT

For the investigation of soft tissues or tissues consisting of soft and hard tissues on the microscopic level, hard X-ray phase tomography has become one of the most suitable imaging techniques. Besides other phase contrast methods grating interferometry has the advantage of higher sensitivity than inline methods and the quantitative results. One disadvantage of the conventional double-grating setup (XDGI) compared to inline methods is the limitation of the spatial resolution. This limitation can be overcome by removing the analyser grating resulting in a single-grating setup (XSGI). In order to verify the performance of XSGI concerning contrast and spatial resolution, a quantitative comparison of XSGI and XDGI tomograms of a human nerve was performed. Both techniques provide sufficient contrast to allow for the distinction of tissue types. The spatial resolution of the two-fold binned XSGI data set is improved by a factor of two in comparison to XDGI which underlies its performance in tomography of soft tissues. Another application for grating-based X-ray phase tomography is the simultaneous visualization of soft and hard tissues of a plaque-containing coronary artery. The simultaneous visualization of both tissues is important for the segmentation of the lumen. The segmented data can be used for flow simulations in order to obtain information about the three-dimensional wall shear stress distribution needed for the optimization of mechano-sensitive nanocontainers used for drug delivery.

Keywords: X-ray phase tomography, double-grating interferometry, single-grating interferometry, laboratory X-ray source, human nerves, human cartilage

1. INTRODUCTION

For investigations of objects in the field of biomedical engineering a three-dimensional, non-destructive imaging technique with a spatial resolution on the cellular level or even below is essential. Most of the questions related to strongly X-ray absorbing species (e.g. bony tissues, teeth, implants,...) can be solved by conventional absorption contrast microtomography using laboratory sources (μ CT) or synchrotron radiation (SR μ CT) [1–6]. For investigations of soft tissues or objects containing soft and hard tissues on the microscopic level phase-contrast microtomography (PC μ CT) is especially suitable. During the last five decades approaches with different principles were introduced to measure the phase shifts of X-ray waves penetrating the specimen. A direct measurement of the phase shift can be performed by a crystal interferometer [7] which was used for the measurements of a mouse kidney [8] or a rat cerebellum [9]. With the advantage of simplicity (no additional optical components) inline phase contrast [10, 11] belongs to a frequently used method. Using a single distance phase retrieval [12] or the more demanding, quantitative holotomography [13] were successfully used for the visualization of a mouse tumor and a rat heart [14]. Using a crystal analyser between the specimen and detector analyser-based imaging (ABI) a third technique which uncovers the phase shift of X rays induced by the specimen [15, 16]. Since its development beginning of the 21st century [17, 18], X-ray grating interferometry, which measures the first derivative of the phase shift (i.e. deflection angle of oncoming X rays), became more and more popular. The main advantages of the quantitative method is its high sensitivity (detection of deflection angles of a few tens nanoradians) which allowed the label-free visualization of individual Purkinje cells surrounded by soft tissue [19], the cm-sized field of view allowing the visualization of brain parts, like the human thalamus [20] and the possibility to use it in laboratory environments [21].

Further author information: (Send correspondence to G.S.) E-mail: georg.schulz@unibas.ch, Telephone: +41 61 207 54 37, Fax: +41 61 207 54 99; www.bmc.unibas.ch

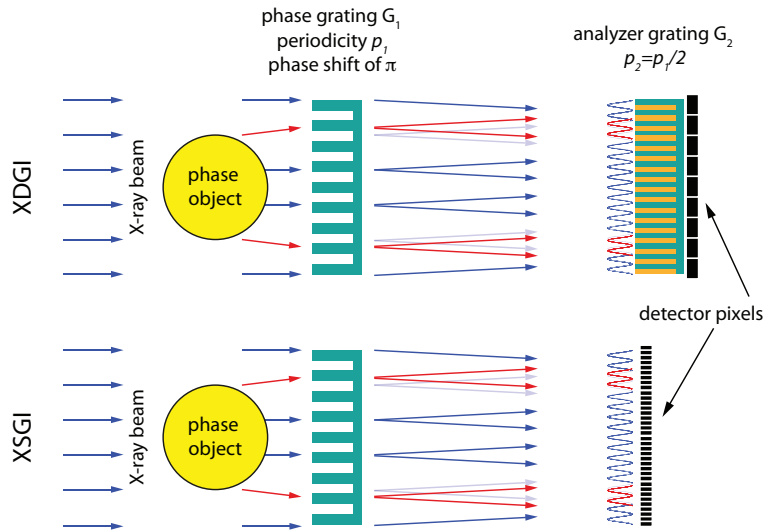


Figure 1. Principles of double- and single-grating interferometer. An interference pattern is generated by the phase grating G_1 . Incoming X rays are deflected by the specimen due to the refractive index differences. The deflection angles of the X rays can be measured by analyzing the distortion of the interference pattern. In most cases the detector pixel size is insufficient to detect the spatial shifts of the pattern. In these cases, an analyzer grating combined with the phase-stepping method is used for the detection. If the pixel size is small enough, the G_2 is not needed and the detection of the deflection angles can be performed by the detector itself.

2. SINGLE-GRATING X-RAY INTERFEROMETER

2.1 Development of a single-grating X-ray interferometer

Using a grating interferometer, the detection of the deflection angle is performed by analyzing the interference pattern of the first grating G_1 . An object between the source and the detector induces slight spatial shifts of the pattern. In most cases, the pixel sizes are larger than the period of the interference pattern. Therefore, an analyzer grating G_2 is used to detect the distortions (Fig. 1 top). One of the disadvantages of such a double-grating interferometer (XDGI) is that, besides the limitations of the detection system, the spatial resolution is limited to twice the analyzer grating period p_2 [22]. This limit can be overcome by directly resolving the interference pattern by the detector (Fig. 1 bottom). Another advantage of a single-grating interferometer (XSGI) is that the phase retrieval can be performed without the need of the phase-stepping method [23] resulting in faster acquisition times and lower dose for the specimen. Other advantages are easier handling, as only one grating has to be aligned, and the related cost reduction. The proof-of-principle of a single-grating interferometer was reported by Takeda *et al.* about ten years ago [24]. Besides the feasibility of the approach the authors show first tomographic results of a two-component polymer with a field of view (FOV) of 1.3 mm^2 . Recent detector developments even allow a sub-pixel precise detection of the interference pattern [25–27]. Although the concept of XSGI is well known and the proof-of-principle was shown ten years ago, only a few manuscripts investigating questions in the field of biomedical engineering can be found. The main reason for that are the limited FOVs of XSGI documented in literature which make preclude the visualization of centimeter-sized specimens. Nowadays, detection systems with 20 or even 40 Megapixel resolutions are available which make XSGI more interesting for biomedical specimens [28, 29].

2.2 Quantitative comparison of XSGI with XDGI

Due to the limited number of publications on XSGI of biomedical specimen, the question arises if the not yet common XSGI is competitive compared with the well-established XDGI. Therefore, a quantitative comparison, similar to the study between holotomography and grating interferometry [30], was performed [29]. The interference pattern of the phase grating could directly be detected by a detection system recently manufactured at the Institute for Data Processing and Electronics (KIT, Germany) which takes advantage of a CMOS chip (CMOSIS,

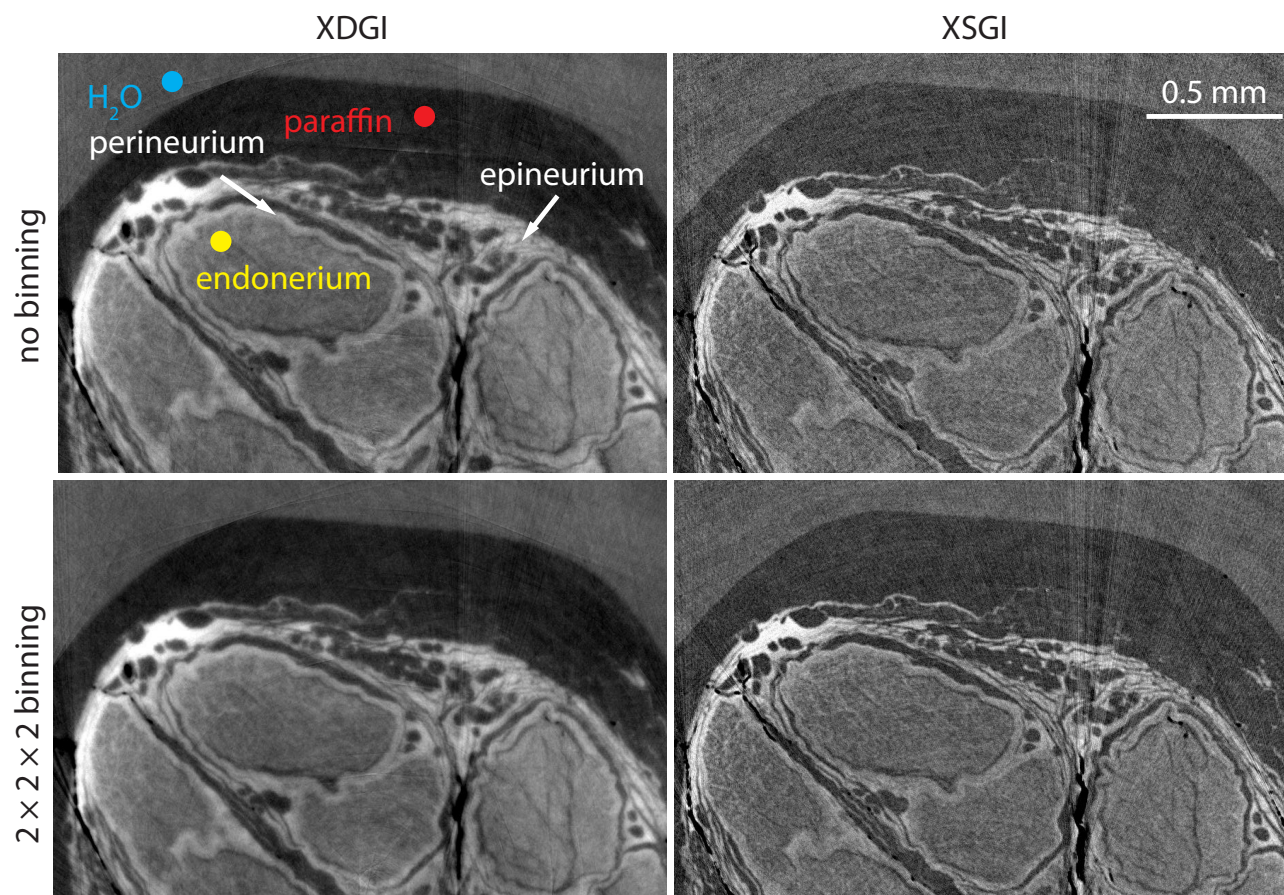


Figure 2. Selected registered slices of XDGI and XSGI without binning and with a binning factor of two.

Antwerp, Belgium) with 5120×3840 pixels (pixel length of $6.4 \mu\text{m}$). Using a magnification of five the effective pixel size was $1.3 \mu\text{m}$ resulting in a relatively large FOV of around $6.7 \times 5.0 \text{ mm}^2$. The experiments at the beamline P07 (PETRA III, DESY, Hamburg, Germany, operated by Helmholtz Zentrum Geesthacht) [31] were performed on a human peripheral nerve embedded in paraffin. The XDGI experiments were performed using a π -shifting phase grating with a periodicity of $4.8 \mu\text{m}$ in combination with an analyzer grating having a periodicity of $2.4 \mu\text{m}$ and $100 \mu\text{m}$ Au structure height. For the XSGI experiments a $\pi/2$ -shifting grating with a periodicity of $4.8 \mu\text{m}$ was used. In order to obtain comparable sensitivities of the two methods the intergrating distance of XDGI had to be half the distance between the grating and detector of XSGI. Taking into account that the relative visibilities should be comparable, the intergrating distance was chosen to 248 mm (\sim third fractional Talbot order) and the distance between grating and detector (XSGI) to 496 mm (\sim first fractional Talbot order). A more precise description of the setup and parameters can be found in literature [29].

The internal structures of the peripheral nerve, namely endoneurium, perineurium and epineurium shown in Fig. 2, can be visualized by both methods. In order to analyze the influence of binning on the quality of the data sets, the spatial resolution and the contrast-to-noise ratio (CNR) were calculated for both cases with binning factor values up to 12. For a combination of spatial resolution and CNR a quality factor was introduced analogously to absorption contrast [32]. For both methods maximal values of the quality factor were present for a binning factor of two. This result can be observed by comparing the unbinned and binned data in Fig. 2. The detection limit of the density deviation was estimated to be around 7 mg/cm^3 for XDGI and around 23 mg/cm^3 for XSGI. XSGI had an improved spatial resolution by a factor of two. If despite the three times lower contrast all the internal structures of the object can be visualized, as it was in our case, XSGI is preferable to XDGI.

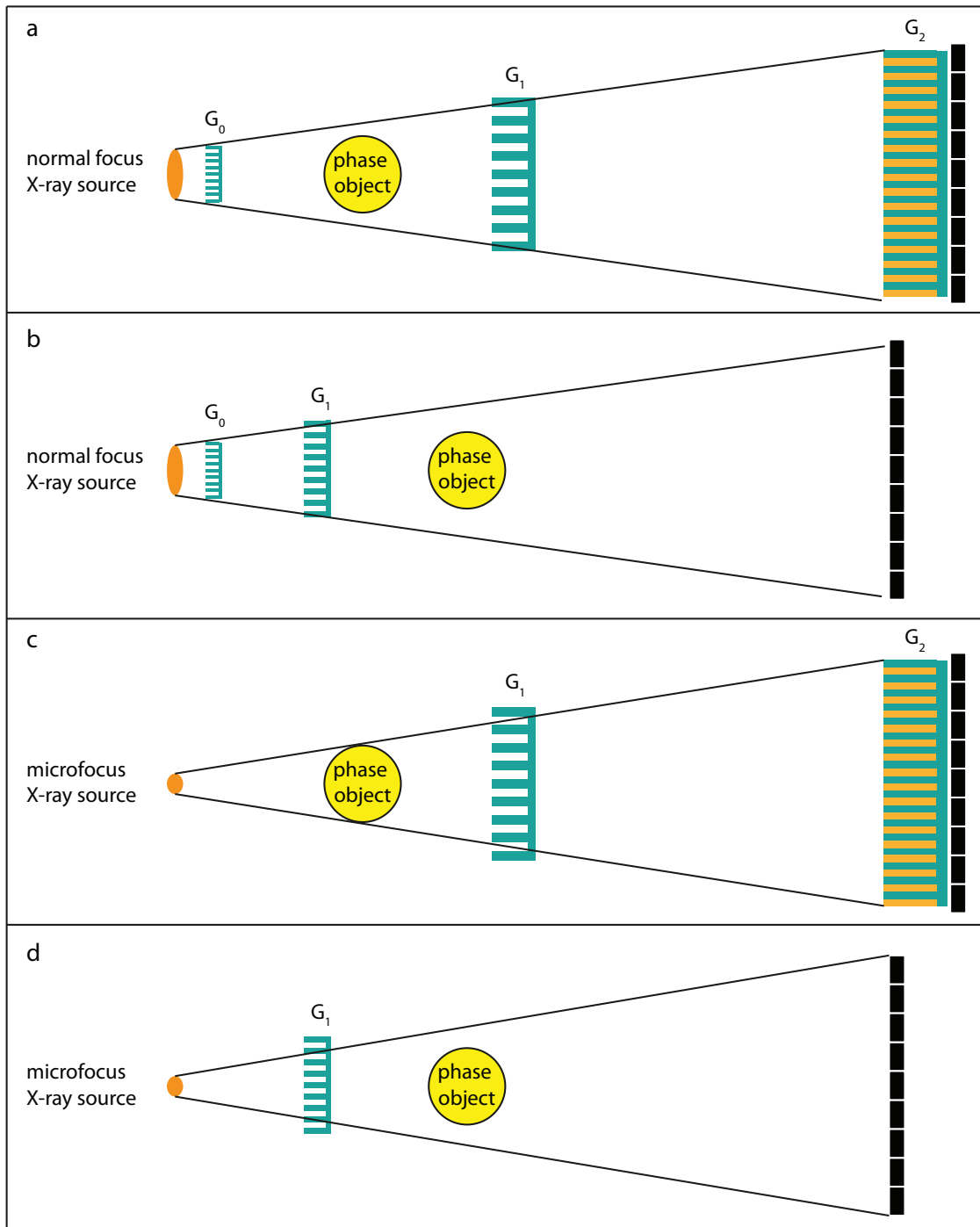


Figure 3. Principles of double- and single-grating interferometer with and without a source grating.

3. GRATING INTERFEROMETRY IN LABORATORY ENVIRONMENT

3.1 Low-brilliance X-ray sources and microfocus X-ray tubes

One of the main advantages of phase tomography using an X-ray interferometer is the possibility to use it in laboratory environment. The required spatial coherence of the X-ray source can be generated by a source grating G_0 as shown in Fig. 3 a) (X-ray Talbot-Lau interferometer) [21]. It was demonstrated that quantitative values

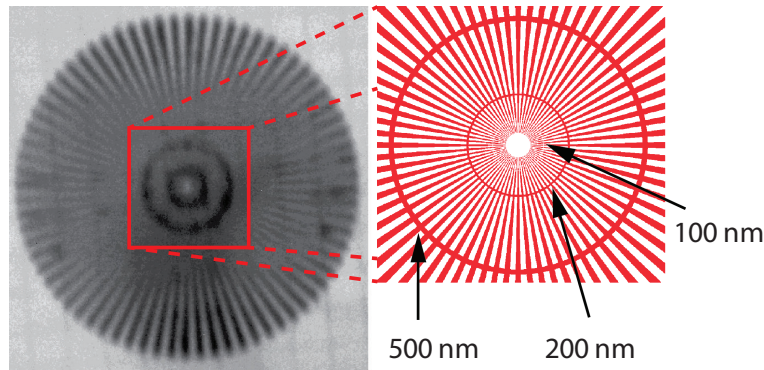


Figure 4. Radiograph of a Siemens star (left) with periodicity at the edge of $2 \mu\text{m}$ and inner feature sizes shown in the schematic (right).

can be achieved despite the polychromatic X-ray spectrum generated by laboratory sources [33]. The method was successfully applied for the visualization of a human hand [34], a chicken heart [35], breast tissues [36, 37] and a human cerebellum piece [38]. After moving grating interferometry from synchrotron to the laboratory, the next step would be the realization of the technique in a hospital. A first step towards that was done by Momose et al. [39] by realizing a clinical phase contrast radiograph for diagnosis of joint diseases and breast cancer, by Tapfer et al. with the installation of the first preclinical phase-contrast mouse CT scanner [40] where radiographs of living animals were acquired and by Gromann et al. with the first X-ray dark-field radiographs of a pig [41].

Taking advantage of the magnification in cone-beam geometry and a sufficient spatial resolution of the detector the interference pattern of grating G_1 can be directly resolved. Then, the analyzer grating G_2 can be removed (X-ray Lau interferometer) shown in Fig. 3 b) [42].

For microfocus X-ray tubes [43, 44] with coherence lengths around the periodicity of G_1 or larger the source grating can be removed. In this case an grating interferometer consisting of two gratings (X-ray Talbot interferometer) comparable to the interferometers used at synchrotron radiation facilities, shown in Fig. 3 c) can be realized [45]. If furthermore, the detector pixel size is sufficient to resolve the fringes directly, G_2 is not needed and an X-ray grating interferometer with one grating in laboratory environment is feasible.

3.2 Implementation of a grating interferometer into commercial μCT scanner

Most of the commercial μCT -systems available are operated in conventional absorption contrast mode. Bruker microCT manufactured the first grating-based phase-contrast desk-top X-ray microtomograph SkyScan 1294 [46] which is a pure phase-contrast microtomography system. An extension of commercially available absorption contrast μCT -system by an add-on X-ray grating interferometer would be beneficial. Depending on the specimen and the information required the system can then be used in absorption- or phase-contrast mode.

For the realization of an X-ray grating interferometer as an add-on device within a commercial μCT -system, enough space between the X-ray source and the detector is needed. The μCT -system available at the Biomaterials Science Center nanotom[®] m (phoenix|x-ray, GE Sensing & Inspection Technologies GmbH, Wunstorf, Germany) for ex-vivo measurements has a variable focus - detector distance between 225 and 600 mm which makes an implementation feasible.

With $100 \mu\text{m}$ pixel size of the detector, the interference pattern of a grating with a periodicity of a few micrometers cannot be resolved directly. This means that an analyzer grating is required. The next step to decide was the necessity of the source grating, i.e. a Talbot-Lau interferometer has to be built or if the spatial coherence is adequate to build a Talbot interferometer consisting of two gratings. The source sizes of the nanofocus X-ray tube are given by the manufacturer to be: $2.7 \mu\text{m}$ (mode 0), $2.0 \mu\text{m}$ (mode 1), $1.0 \mu\text{m}$ (mode 2) and $0.9 \mu\text{m}$ (mode 3). In order to confirm these values measurements of a Siemens star from Laboratory for Micro and Nanotechnology (Paul Scherrer Institute, Villigen, Switzerland) were performed. The radiograph in

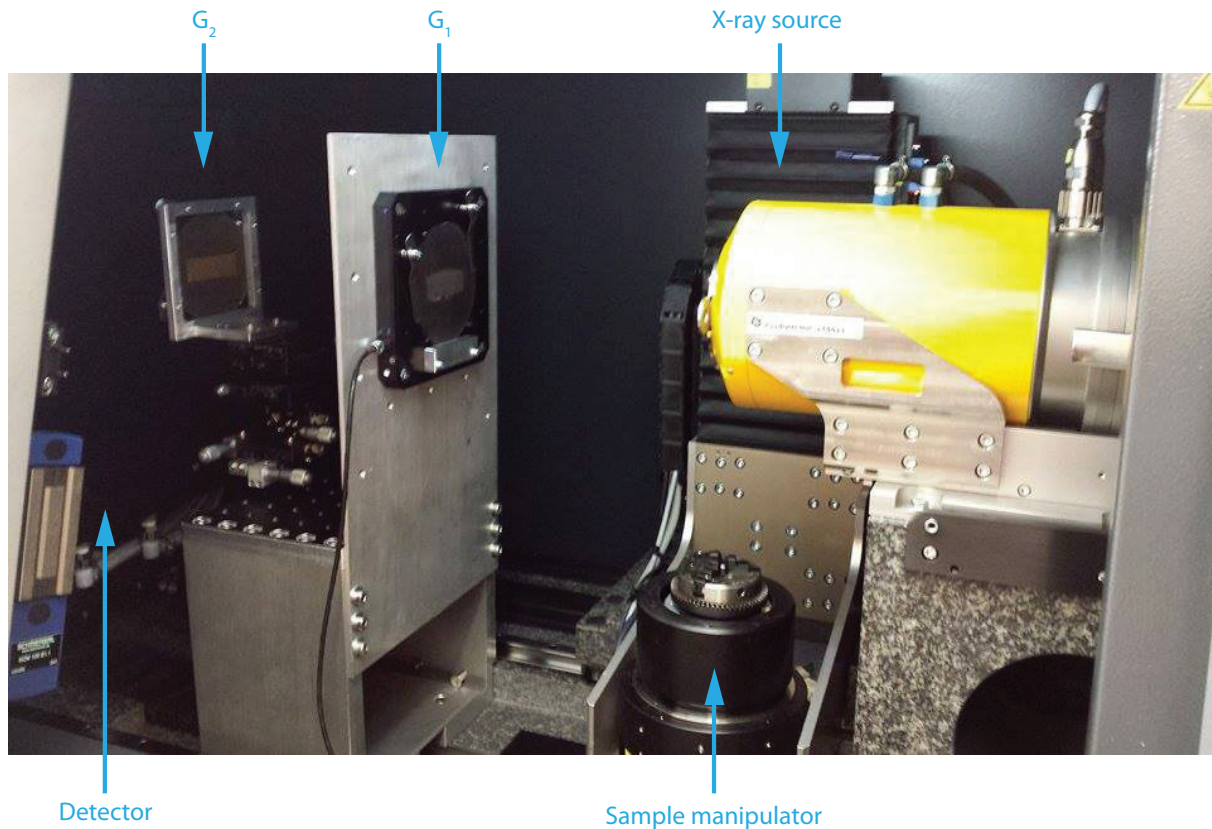


Figure 5. View of the μ CT-system interior containing the Talbot grating interferometer.

(Fig. 4) shows results acquired in mode 3 with an acceleration voltage of 40 kV and a beam current of 640 μ A. Looking at the radiograph a source size of around 1 μ m could be estimated which confirms the specifications of the manufacturer. The spatial coherence is sufficient to realize a Talbot interferometer without a source grating.

The grating interferometer inside the nanotom is shown in Fig. 5. For tomographic acquisition the specimen is mounted on the rotation stage between source and interferometer. For the phase-stepping of the grating a P-540-series XY piezo scanning stage (PI GmbH, Karlsruhe, Germany) with an aperture of 80×80 mm² and a travel range of 200 μ m in x - and y -direction was integrated. The alignment of the second grating is performed by a motorized goniometer stage MOG-65-15 and a manual XYZ stage (Optics Focus, Beijing, China). The interferometer consisted of a phase grating G_1 with a periodicity of 7 μ m and a Au structure height of 6 μ m inducing a phase shift of π for X rays with an energy of 30 keV. The analyzer grating had a periodicity of 7 μ m and a Au structure height of 85 μ m. Both gratings were fabricated by microworks (Karlsruhe, Germany). The symmetric setup with a distance of 296 mm between source and G_1 and between the two gratings (first fractional Talbot distance) was operating using an acceleration voltage of 42 kV and a beam current of 275 μ A (mode 1). The space between source and G_1 (where the rotation stage is located) allows effective pixel sizes between 1 and 40 μ m. A more detailed description of the setup can be found in literature [47].

The quality of a grating interferometer can be quantified by the visibility defined by

$$V = \frac{I_{max} - I_{min}}{I_{max} + I_{min}}$$

where I_{max} and I_{min} are the maximal and minimal values of the stepping curve. Using the interferometer a homogeneous region of around 3×6 cm² with an average visibility of 25 % could be achieved. The first measurements were performed on a formalin-fixed cylinder (around 5 mm diameter) of a human femur containing bone and cartilage. For each projection seven phase stepping images were acquired over two periods of the

interference pattern with an exposure time of 10 s per image. With 600 projections over 360 the resulting scanning time was 17 h. The results were then compared with a data set acquired with the nanotom m in the conventional absorption contrast mode with regard to the spatial resolution and the contrast-to-noise ratio between formalin and cartilage. Whereas the data sets showed a comparable spatial resolution, the contrast-to-noise ratio of the phase contrast data set was increased by a factor of four which allowed to differentiate between cartilage and formalin.

4. DISCUSSION

Phase tomography has become the method of choice to visualize the micro- and nanostructures of objects composed of elements with low atomic numbers including human and animal tissues [19, 48], polymer blends [49], and low-X-ray absorbing scaffolds [50]. It is also powerful to visualize low-absorbing components in the vicinity of strongly absorbing species [51], as the tissues around metallic and ceramic implants, since the real part of the refractive index is a linear function of the atomic number and the X-ray absorption scales with the power law [52].

Therefore, it is not surprising that the expert users with challenging tasks more frequently apply phase-contrast approaches. As the single-distance phase retrieval at synchrotron radiation facilities is simple and provides data with submicron resolution easily, this approach is especially popular. The obtained quantities, however, have to be regarded with care, because the assumptions to be made are often questionable. Here, the grating-based tomography, which belongs to the phase tomography methods developed most recently, are more reliable. One can find the experimental setups at synchrotron radiation facilities and in the laboratories of the expert teams [53, 54]. Whereas most of the grating interferometers at synchrotron radiation facilities are composed of two gratings, the lab setups often rely on three gratings. Because the detectors are steadily improved with respect to pixel numbers and pixel size, the incorporation of the analyzer grating is not necessary any more. The performance of a single-grating setup with respect to the double grating interferometer has been demonstrated in detail very recently [29, 55].

Simultaneously, the spatial resolution of phase tomography data has been pushed to well below the optical limit, i.e. to the nanometer range below 100 nm incorporating X-ray optics. This development brings many details on the nanometer scale to light, but increases the size of the datasets considerably and reduces the field of view to the submillimeter range. Characteristic examples are also given in the present volume [56, 57].

The high sensitivity of phase tomography increases the chance to recognize artefacts. For example, in Fig. 2 one finds streak artefacts in the XSGI slice. Ring artefacts can become critical and, thus, the compensation is a prerequisite for segmentation purposes. For a tumor with surrounding healthy tissue, for example, P. Thalmann et al. [58] proposed a powerful procedure to accurately segment the brain tumor.

ACKNOWLEDGMENTS

The authors thank H. Deyhle from University of Basel, and F. Beckmann from Helmholtz-Zentrum Geesthacht for the help with the measurements and many useful discussions and C. Bikis from University of Basel, J. Hench and G. Schweighauser of the Neuropathology Department of the Basel University Hospital for providing the sample and the special preparation required for tomography. The project was partially funded by Swiss National Science Foundation (R'equip initiative 133802 and SNF projects 147172 and 144535.).

REFERENCES

- [1] Yu, B., Langer, M., Pacureanu, A., Gauthier, R., Follet, H., Mitton, D., Olivier, C., Cloetens, P., and Peyrin, F., "Assessment of imaging quality in magnified phase CT of human bone tissue at the nanoscale," *Proc. SPIE* **10391**, 103910L (2017).
- [2] Davis, G. and Mills, D., "High-contrast X-ray microtomography in dental research," *Proc. SPIE* **10391**, 1039119 (2017).

- [3] Moosmann, J., Zeller-Plumhoff, B., Wieland, D. C. F., Galli, S., Krüger, D., Dose, T., Burmester, H., Wilde, F., Bech, M., Peruzzi, N., Wiese, B., Hipp, A., Beckmann, F., Hammel, J., and Willumeit-Römer, R., “Biodegradable magnesium-based implants in bone studied by synchrotron radiation microtomography,” *Proc. SPIE* **10391**, 103910O (2017).
- [4] Mani-Caplazi, G., Schulz, G., Deyhle, H., Hotz, G., Vache, W., Wittwer-Backofen, U., and Müller, B., “Imaging of the human tooth cementum ultrastructure of archeological teeth using hard X-ray microtomography to determine age-at-death and stress periods,” *Proc. SPIE* **10391**, 103911C (2017).
- [5] Costeur, L., Mennecart, B., Khimchenko, A., Müller, B., and Schulz, G., “Innervation of the cow’s inner ear derived from micro-computed tomography,” *Proc. SPIE* **10391**, 103911I (2017).
- [6] Kwan, C. C., Tan, X., Stock, S. R., Soriano, C., Xiao, X., and Richter, C.-P., “Microanatomy of the cochlear hook,” *Proc. SPIE* **10391**, 103910B (2017).
- [7] Bonse, U. and Hart, M., “An X-ray interferometer,” *Appl. Phys. Lett.* **6**, 155–156 (1965).
- [8] Beckmann, F., Bonse, U., Busch, F., Günnewig, O., and Biermann, T., “A novel system for X-ray phase-contrast microtomography,” *Hasylab Annu. Rep.* **2**, 691–692 (1995).
- [9] Momose, A. and Fukuda, J., “Phase-contrast radiographs of nonstained rat cerebellar specimen,” *Med. Phys.* **22**, 375–379 (1995).
- [10] Snigirev, A. A., Snigireva, I., Kohn, V., Kuznetsov, S., and Schelokov, I., “On the possibilities of x-ray phase contrast microimaging by coherent high-energy synchrotron radiation,” *Rev. Sci. Instrum.* **66**, 5486–5492 (1995).
- [11] Cloetens, P., Barrett, R., Baruchel, J., Guigay, J.-P., and Schlenker, M., “Phase objects in synchrotron radiation hard X-ray imaging,” *J. Phys. D: Appl. Phys.* **29**, 133–146 (1996).
- [12] Paganin, D., Mayo, S. C., Gureyev, T. E., Miller, P. R., and Wilkins, S. W., “Simultaneous phase and amplitude extraction from a single defocused image of a homogeneous object,” *J. Microsc.* **206**, 33–40 (2002).
- [13] Cloetens, P., Ludwig, W., Baruchel, J., Van Dyck, D., Van Landuyt, J., Guigay, J. P., and Schlenker, M., “Holotomography: quantitative phase tomography with micrometer resolution using hard synchrotron radiation X-rays,” *Appl. Phys. Lett.* **75**, 2912–2914 (1999).
- [14] Lang, S., Zanette, I., Dominietto, M., Langer, M., Rack, A., Schulz, G., Le Duc, G., David, C., Mohr, J., Pfeiffer, F., Müller, B., and Weitkamp, T., “Experimental comparison of grating- and propagation-based hard X-ray phase tomography of soft tissue,” *J. Appl. Phys.* **116**, 154903 (2014).
- [15] Förster, E., Goetz, K., and Zaumseil, P., “Double crystal diffractometry for the characterization of targets for laser fusion experiments,” *Krist. Tech.* **15**, 937–945 (1980).
- [16] Davis, T. J., Gao, D., Gureyev, T. E., Stevenson, A. W., and Wilkins, S., “Phase-contrast imaging of weakly absorbing materials using hard X-rays,” *Nature* **373**, 595–598 (1995).
- [17] David, C., Nöhammer, B., Solak, H. H., and Ziegler, E., “Differential X-ray phase contrast imaging using a shearing interferometer,” *Appl. Phys. Lett.* **81**, 3287–3289 (2002).
- [18] Momose, A., Kawamoto, S., Koyama, I., Hamaishi, Y., Takai, K., and Suzuki, Y., “Demonstration of X-ray Talbot interferometry,” *Jpn. J. Appl. Phys.* **42**, 866–868 (2003).
- [19] Schulz, G., Weitkamp, T., Zanette, I., Pfeiffer, F., Beckmann, F., David, C., Rutishauser, S., Reznikova, E., and Müller, B., “High-resolution tomographic imaging of a human cerebellum: Comparison of absorption and grating based phase contrast,” *J. R. Soc. Interface* **7**, 1665–1676 (2010).
- [20] Schulz, G., Morel, A., Imholz, M. S., Deyhle, H., Weitkamp, T., Zanette, I., Pfeiffer, F., David, C., Müller-Gerbl, M., and Müller, B., “Evaluating the microstructure of human brain tissues using synchrotron radiation-based micro computed tomography,” *Proc. SPIE* **7804**, 78040F (2010).
- [21] Pfeiffer, F., Weitkamp, T., Bunk, O., and David, C., “Phase retrieval and differential phase-contrast imaging with low-brilliance X-ray sources,” *Nature Phys.* **2**, 258–261 (2006).
- [22] Weitkamp, T., Diaz, A., David, C., Pfeiffer, F., Stampanoni, M., Cloetens, P., and Ziegler, E., “X-ray phase imaging with a grating interferometer,” *Opt. Express* **13**, 6296–6304 (2005).
- [23] Wang, Z., Huang, Z., Zhang, L., Kang, K., and Zhu, P., “Fast X-ray phase-contrast imaging using high resolution detector,” *IEEE Trans. Nucl. Sci.* **56**, 1383–1388 (2009).

- [24] Takeda, Y., Yashiro, W., Suzuki, Y., Aoki, S., Hattori, T., and Momose, A., "X-ray phase imaging with single phase grating," *Jpn. J. Appl. Phys.* **46**, L89 (2007).
- [25] Krejci, F., Jakubek, J., and Kroupa, M., "Hard x-ray phase contrast imaging using single absorption grating and hybrid semiconductor pixel detector," *Rev. Sci. Instrum.* **81**, 113702 (2010).
- [26] Cartier, S., Kagias, M., Bergamaschi, A., Wang, Z., Dinapoli, R., Mozzanica, A., Ramilli, M., Schmitt, B., Brückner, M., Fröjdh, E., Greiffenberg, D., Mayilyan, D., Mezza, D., Redford, S., Ruder, C., Schädler, L., Shi, X., Thattil, D., Tinti, G., Zhanga, J., and Stampanoni, M., "Micrometer-resolution imaging using MÖNCH: towards G₂-less grating interferometry," *J. Synchrotron Rad.* **23**, 1462–1473 (2016).
- [27] Kagias, M., Cartier, S., Wang, Z., Bergamaschi, A., Dinapoli, R., Mozzanica, A., Schmitt, B., and Stampanoni, M., "Single shot x-ray phase contrast imaging using a direct conversion microstrip detector with single photon sensitivity," *Appl. Phys. Lett.* **108**, 234102 (2016).
- [28] Zdora, M.-C., Vila-Comamala, J., Schulz, G., Khimchenko, A., Hipp, A., Cook, A. C., Dilg, D., David, C., Grünzweig, C., Rau, C., Thibault, P., and Zanette, I., "X-ray phase microtomography with a single grating for high-throughput investigations of biological tissue," *Biomed. Opt. Express* **8**, 1257–1270 (2017).
- [29] Thalmann, P., Bikis, C., Hipp, A., Müller, B., Hieber, S. E., and Schulz, G., "Single and double grating-based X-ray microtomography using synchrotron radiation," *Appl. Phys. Lett.* **110**, 061103 (2017).
- [30] Zanette, I., Lang, S., Rack, A., Dominietto, M., Langer, M., Pfeiffer, F., Weitkamp, T., and Müller, B., "Holotomography versus X-ray grating interferometry: a comparative study," *Appl. Phys. Lett.* **103**, 244105 (2013).
- [31] Hipp, A., Beckmann, F., Lytaev, P., Greving, I., Lottermoser, L., Dose, T., Kirchhof, R., Burmester, H., Schreyer, A., and Herzen, J., "Grating-based X-ray phase-contrast imaging at PETRA III," *Proc. SPIE* **9212**, 921206 (2014).
- [32] Thurner, P., Beckmann, F., and Müller, B., "An optimization procedure for spatial and density resolution in hard X-ray micro-computed tomography," *Nucl. Instrum. Methods Phys. Res., Sect. B* **225**, 599–603 (2004).
- [33] Herzen, J., Donath, T., Pfeiffer, F., Bunk, O., Padeste, C., Beckmann, F., Schreyer, A., and David, C., "Quantitative phase-contrast tomography of a liquid phantom using a conventional x-ray tube source," *Opt. Express* **17**, 10010–10018 (2009).
- [34] Donath, T., Pfeiffer, F., Bunk, O., Grünzweig, C., Hempel, E., Popescu, S., Vock, P., and David, C., "Toward clinical X-ray phase-contrast CT: Demonstration of enhanced soft-tissue contrast in human specimen," *Invest. Radiol.* **45**, 445–452 (2010).
- [35] Bech, M., Jensen, T. H., Feidenhans'l, R., Bunk, O., David, C., and Pfeiffer, F., "Soft-tissue phase-contrast tomography with an x-ray tube source," *Phys. Med. Biol.* **54**, 2747–2753 (2009).
- [36] Willner, M., Herzen, J., Grandl, S., Auweter, S., Mayr, D., Hipp, A., Chabior, M., Sarapata, A., Achterhold, K., Zanette, I., Weitkamp, T., Sztrokay, A., Hellerhoff, K., Reiser, M., and Pfeiffer, F., "Quantitative breast tissue characterization using grating-based x-ray phase-contrast imaging," *Phys. Med. Biol.* **59**, 1557–1571 (2014).
- [37] Grandl, S., Willner, M., Herzen, J., Sztrokay-Gaul, A., Mayr, D., Auweter, S. D., Hipp, A., Birnbacher, L., Marschner, M., Chabior, M., Reiser, M., Pfeiffer, F., Bamberg, F., and Hellerhoff, K., "Visualizing typical features of breast fibroadenomas using phase-contrast CT: An ex-vivo study," *PLOS ONE* **9**, e9710 (2014).
- [38] Birnbacher, L., Willner, M., Velroyen, A., Marschner, M., Hipp, A., Meiser, J., Koch, F., Schrter, T., Kunka, D., Mohr, J., Pfeiffer, F., and Herzen, J., "Experimental realisation of high-sensitivity laboratory X-ray grating-based phase-contrast computed tomography," *Sci. Rep.* **6**, 24022 (2016).
- [39] Momose, A., Yashiro, W., Kido, K., Kiyohara, J., Makifuchi, C., Ito, T., Nagatsuka, S., Honda, C., Noda, D., Hattori, T., Endo, T., Nagashima, M., and Tanaka, J., "X-ray phase imaging: from synchrotron to hospital," *Phil. Trans. R. Soc. A* **372**, 20130023 (2014).
- [40] Tapfer, A., Bech, M., Velroyen, A., Meiser, J., Mohr, J., Walter, M., Schulz, J., Pauwels, B., Bruyndonckx, P., Liu, X., Sasov, A., and Pfeiffer, F., "Experimental results from a preclinical X-ray phase-contrast CT scanner," *PNAS* **109**, 15691–15696 (2012).

- [41] Gromann, L. B., De Marc, F., Willer, K., Noël, P., Scherer, K., Renger, B., Gleich, B., Achterhold, K., Fingerle, A. A., Muenzel, D., Auweter, S., Hellbach, K., Reiser, M., Baehr, A., Dmochewicz, M., Schroeter, T. J., Koch, F. J., Meyer, P., Kunka, D., Mohr, J., Yaroshenko, A., Maack, H.-I., Pralow, T., van der Heijden, H., Proksa, R., Koehler, T., Wieberneit, N., Rindt, K., Rummeny, E. J., Pfeiffer, F., and Herzen, J., “In-vivo X-ray dark-field chest radiography of a pig,” *Sci. Rep.* **7**, 4807 (2017).
- [42] Momose, A., Kuwabara, H., and Yashiro, W., “X-ray phase imaging using Lau effect,” *Appl. Phys. Express* **4**, 066603 (2011).
- [43] Yoon, K.-H., Ryu, J., Jung, C., Ryu, C., Kim, Y., Kwon, Y., Park, M., Cho, S., and Chon, K., “Differential X-ray phase-contrast imaging with a grating interferometer using a laboratory X-ray micro-focus tube,” *J. Korean Phys. Soc.* **65**, 2111–2116 (2014).
- [44] Zhou, T., Lundström, U., Thüring, T., Rutishauser, S., Larsson, D., Stampanoni, M., David, C., Hertz, H., and Burvall, A., “Comparison of two x-ray phase-contrast imaging methods with a microfocus source,” *Opt. Express* **21**, 30183–30195 (2013).
- [45] Thuering, T., Modregger, P., Grund, T., Kenntner, J., David, C., and Stampanoni, M., “High resolution, large field of view x-ray differential phase contrast imaging on a compact setup,” *Appl. Phys. Lett.* **99**, 041111 (2011).
- [46] Gusenbauer, C., Leiss-Holzinger, E., Senck, S., Mathmann, K., Kastner, J., Hunger, S., and Birkfellner, W., “Characterization of medical and biological samples with a Talbot-Lau grating interferometer μ XCT in comparison to reference methods,” *Case Stud. Nondestr. Test. Eval.* **6**, 30–38 (2016).
- [47] Khimchenko, A., Schulz, G., Deyhle, H., Hieber, S. E., Hasan, S., Bikis, C., Schulz, J., Costeur, L., and Müller, B., “Non-destructive phase contrast hard X-ray imaging to reveal the three-dimensional microstructure of soft and hard tissues,” *Proc. SPIE* **9797**, 97970B (2016).
- [48] Pfeiffer, F., David, C., Bunk, O., Poitry-Yamate, C., Grütter, R., Müller, B., and Weitkamp, T., “High-sensitivity phase-contrast tomography of rat brain in phosphate buffered saline,” *J. Phys. Conf. Ser.* **186**, 0120461–0120463 (2009).
- [49] Wu, Y., Takano, H., and Momose, A., “In-situ observation of polymer blend phase separation by X-ray Talbot-Lau interferometer,” *Proc. SPIE* **10391**, 103910E (2017).
- [50] Langer, M., Liu, Y., Tortelli, F., Cloetens, P., Cancedda, R., and Peyrin, F., “Regularized phase tomography enables study of mineralized and unmineralized tissue in porous bone scaffold,” *J. Microsc.* **238**, 230–239 (2010).
- [51] Holme, M. N., Schulz, G., Deyhle, H., Weitkamp, T., Beckmann, F., Lobrinus, J. A., Rikhtegar, F., Kurtcuoglu, V., Zanette, I., Saxer, T., and Müller, B., “Complementary X-ray tomography techniques for histology-validated 3D imaging of soft and hard human tissues using plaque-containing blood vessels as examples,” *Nature Prot.* **9**, 1401–1415 (2014).
- [52] Bonse, U. and Busch, F., “X-ray computed microtomography (μ CT) using synchrotron radiation (SR),” *Prog. Biophys. molec. Biol.* **65**, 133–169 (1996).
- [53] Balles, A., Dittman, J., Fella, C., Zabler, S., and Hanke, R., “Quantitative phase contrast and X-ray scattering micro-tomography with the 9.2 keV liquid metal jet anode - applications on materials and life science,” *Proc. SPIE* **10391**, 1039109 (2017).
- [54] Momose, A., Takano, H., Hoshino, M., Wu, Y., and Vegso, K., “Recent advance in grating-based X-ray phase tomography,” *Proc. SPIE* **10391**, 103910Y (2017).
- [55] Hipp, A., Moosmann, J., Herzen, J., Hammel, J. U., Schreyer, A., and Beckmann, F., “High-resolution grating interferometer for phase-contrast imaging at PETRA III,” *Proc. SPIE* **10391**, 1039108 (2017).
- [56] Reichardt, M., Frohn, J., Töpferwien, M., Nicolas, J. D., Markus, A., Alves, F., and Salditt, T., “Nanoscale holographic tomography of heart tissue with x-ray waveguide optics,” *Proc. SPIE* **10391**, 1039105 (2017).
- [57] Takano, H., Wu, Y., and Momose, A., “Development of full-field X-ray phase-tomographic microscope based on laboratory X-ray source,” *Proc. SPIE* **10391**, 1039110 (2017).
- [58] Thalmann, P., Bikis, C., Schulz, G., Paleo, P., Mirone, A., Rack, A., Siegrist, S., Cörek, E., Huwyler, J., and Müller, B., “Removing ring artefacts from synchrotron radiation-based hard X-ray tomography data,” *Proc. SPIE* **10391**, 1039114 (2017).